1 **Real-time monitoring of subcellular H_2O_2 distribution in *Chlamydomonas***
2 ***reinhardtii***

3

4 Justus Niemeyer[1], David Scheuring[2], Julian Oestreicher[3], Bruce Morgan[3,§], and
5 Michael Schroda[1,§]

6

7 Author's institution(s)/affiliation(s)
8 [1] Molekulare Biotechnologie & Systembiologie, TU Kaiserslautern, Paul-Ehrlich
9 Straße 23, D-67663 Kaiserslautern, Germany
10 [2] Phytopathologie, TU Kaiserslautern, Paul-Ehrlich Straße 22, D-67663
11 Kaiserslautern, Germany
12 [3] Institute of Biochemistry, Zentrum für Human- und Molekularbiologie (ZHMB),
13 Saarland University, D-66123 Saarbrücken, Germany.

14

15 § Corresponding authors: Michael Schroda (schroda@bio.uni-kl.de) and Bruce
16 Morgan (bruce.morgan@uni-saarland.de)

17

18 Short title: H_2O_2 dynamics in Chlamydomonas

19

20 The author responsible for distribution of materials integral to the findings presented
21 in this article in accordance with the policy described in the Instructions for Authors
22 (www.plantcell.org) is: Michael Schroda (schroda@bio.uni-kl.de).

23

24

25

26

27

28

29

30

31

1

Abstract

H_2O_2 has been recognized as an important signaling molecule in plants. We sought to establish a genetically encoded, fluorescent H_2O_2 sensor that allows H_2O_2 monitoring in all major subcompartments of a Chlamydomonas cell. To this end we engineered the hypersensitive H_2O_2 sensor, roGFP2-Tsa2ΔC$_R$, as a genetic part for the Chlamydomonas Modular Cloning toolbox. Using previously generated parts, together with new ones, we constructed modules and devices that target the sensor to the cytosol, nucleus, mitochondrial matrix, chloroplast stroma, thylakoid lumen, and ER. The sensor was functional in all compartments, except for the ER where it was fully oxidized. Employing our novel sensors, we show that H_2O_2 produced by photosynthetic linear electron transport (PET) in the stroma leaks into the cytosol but only reaches other subcellular compartments if produced under non-physiological conditions. Our results thus imply the establishment of steep intracellular H_2O_2 gradients under normal physiological conditions and suggest that the cytosolic complement of H_2O_2 scavenging enzymes effectively limits H_2O_2 diffusion. Furthermore, in heat stressed cells, we show that cytosolic H_2O_2 levels closely mirror temperature up- and downshifts and are independent from PET. We anticipate that these sensors will greatly facilitate future investigations into H_2O_2 biology in algal and plant cells.

Introduction

In plant cells, hydrogen peroxide (H_2O_2), or its precursor superoxide, is produced as a side product of cellular processes including photosynthetic linear electron transport (PET), the mitochondrial respiratory chain, or substrate oxidation, for example by the photorespiration enzyme glycolate oxidase (Cheeseman, 2007; Foyer and Noctor, 2016). H_2O_2 is a relatively stable molecule and is largely unreactive with most proteins. It is therefore well-suited as a second messenger in cellular signaling cascades (Waszczak et al., 2018). Such signaling cascades can be fueled either with H_2O_2 produced as a side product, e.g. from PET (Exposito-Rodriguez et al., 2017), or with H_2O_2 produced specifically for a signaling cascade. One example here is the respiratory burst oxidase homolog D (RBOHD) in the plasma membrane that

2

63   produces H_2O_2 for systemic signaling upon stimuli including wounding, cold, heat,
64   high light and salinity (Miller et al., 2009; Lew et al., 2020), and plays a role during
65   ABA-induced stomatal movement (Pei et al., 2000; Kwak et al., 2003).
66
67   The recognition of H_2O_2 as second messenger has generated a demand for tools to
68   measure H_2O_2 dynamics within plant cells. The development of synthetic dyes for
69   H_2O_2 detection has allowed some insights, however, several problems are inherent to
70   their use, including variable uptake and efflux, lack of subcellular compartment
71   specificity, lack of redox species specificity, and the irreversibility of their reaction with
72   H_2O_2 (Bilan and Belousov, 2018; Roma et al., 2018). A major methodological
73   advance in the subcellular detection of H_2O_2 came with the creation of genetically
74   encoded fluorescent protein sensors that allow for subcellular compartment-specific
75   monitoring of H_2O_2 in real time in living organisms. The first of these sensors was
76   HyPer (Belousov et al., 2006). HyPer consists of a circularly permuted YFP
77   positioned between two halves of the H_2O_2-sensitive *E.coli* transcription factor OxyR.
78   The presence of H_2O_2 leads to the formation of a disulfide bond between the H_2O_2-
79   reactive cysteine on one OxyR domain and the resolving cysteine residue on the
80   other domain. This results in a structural change that is transmitted to the cpYFP,
81   thereby inducing a ratiometric change in the fluorescence excitation spectrum, thus
82   allowing measurements that are independent of probe concentration. Several
83   improved versions of HyPer have been generated that expand its dynamic range, its
84   oxidation and reduction rates, or employ a red fluorescent protein (Bilan and
85   Belousov, 2018).
86
87   A second family of genetically encoded fluorescent H_2O_2 sensors is based on
88   roGFP2, which contains two cysteines in adjacent β-strands on the surface of the
89   protein β-barrel (Hanson et al., 2004). The formation of a disulfide bond between
90   these cysteines results in small structural changes that induce a ratiometric change in
91   the fluorescence excitation spectrum. As for HyPer, this allows measurements that
92   are independent of sensor concentration. Since the cysteines of roGFP2 do not
93   readily react with H_2O_2, roGFP2 needs to be coupled with an H_2O_2 reactive enzyme
94   in a redox relay system. The first such sensor was roGFP2-Orp1, which involves a
95   genetic fusion between the glutathione peroxidase-like enzyme Orp1 from budding

3

96   yeast and roGFP2, with a short interspacing polypeptide linker (Gutscher et al.,
97   2009). In this sensor, Orp1 sensitively reacts with H_2O_2 to form an intramolecular
98   disulfide bond between its peroxidatic and resolving cysteine, followed by a thiol-
99   disulfide exchange reaction to roGFP2.
100
101   Many cellular peroxiredoxins contain peroxidatic cysteine residues that react with
102   H_2O_2 2–3 orders of magnitude faster than the Orp1 peroxidase (Roma et al., 2018).
103   This observation led to the generation of roGFP2-Tsa2ΔC_R, a genetic fusion between
104   the yeast typical 2-Cys peroxiredoxin Tsa2 and roGFP2 (Morgan et al., 2016). The
105   resolving cysteine in Tsa2 was mutated to alanine such that reduction of the sensor
106   by thioredoxin is impeded and sensor sensitivity further enhanced. In yeast, this
107   sensor was shown to be approximately 20-fold more sensitive towards H_2O_2 than
108   either HyPer or roGFP2-Orp1 (Morgan et al., 2016). Furthermore, roGFP2-Tsa2ΔC_R
109   makes a negligible contribution to the cellular H_2O_2-scavenging capacity, has a low
110   propensity for hyperoxidation, and is unaffected by changes in pH between 6 and 8.5
111   (Morgan et al., 2016; Roma et al., 2018). Its pH insensitivity distinguishes roGFP2-
112   Tsa2ΔC_R from HyPer, for which additional pH probes need to be implemented to
113   account for changes in pH, as observed for example in the stroma upon illumination
114   (Schwarzlander et al., 2014; Exposito-Rodriguez et al., 2017). A pH-insensitive
115   version of HyPer (HyPer7) has been established recently, but not yet for plant cells
116   (Pak et al., 2020).
117
118   The aim of this work was to establish a sensitive H_2O_2 sensor for the unicellular
119   green alga *Chlamydomonas reinhardtii*, a traditional model system for plant cell
120   biology and photosynthesis (Sasso et al., 2018). To this end, we engineered roGFP2-
121   Tsa2ΔC_R as a genetic part for the Chlamydomonas Modular Cloning (MoClo) toolbox
122   for synthetic biology. We targeted the sensor to six cell compartments – cytosol,
123   nucleus, mitochondrial matrix, chloroplast stroma, thylakoid lumen, and ER and show
124   that changes in H_2O_2 concentrations can be monitored in real time in all
125   compartments, except for the ER. Our data reveal the establishment of strong
126   intracellular H_2O_2 gradients in response to physiological stresses.
127
128

4

129

5

130   **Results**

131   **Construction of an H_2O_2 sensor for Chlamydomonas**

132   To develop a genetically encoded, fluorescent H_2O_2 sensor for *Chlamydomonas*

133   *reinhardtii*, we synthesized the coding sequence of roGFP2-Tsa2ΔC_R (Morgan et al.,

134   2016) with codons optimized for expression in Chlamydomonas and containing the

135   three *RBCS2* introns, as a level 0 part for the Chlamydomonas Modular Cloning

136   (MoClo) kit (Crozet et al., 2018) (Figure 1A). This part was then assembled into level

137   1 modules which included either the *PSAD* promoter or the *HSP70A-RBCS2* fusion

138   promoter (pAR), an *RPL23* terminator, and various N-terminal targeting peptides, C-

139   terminal tags, or retention signals to facilitate localization to defined subcellular

140   compartments. The resulting level 1 modules were then assembled into level 2

141   devices together with a spectinomycin resistance (*aadA*) cassette controlled by the

142   *PSAD* promoter and terminator (Figure 1B). The level 2 devices were then

143   transformed into the UVM4 expression strain (Neupert et al., 2009). As a control, we

144   generated a level 0 part containing only the roGFP2 coding sequence, harboring the

145   first *RBCS2* intron, and placed it under control of the *AR* promoter (roGFP2, Figure

146   1B). The best promoters and targeting peptides to use in Chlamydomonas is still a

147   subject of debate. We therefore tested different promoters and targeting peptide

148   combinations. For each device, at least 13 spectinomycin resistant transformants

149   were picked and screened for sensor expression by immunoblotting. Between 30%

150   and 70% of the transformants expressed the sensor to readily detectable levels

151   (Supplemental Figure 1). To compare the expression levels of the sensors, whole-cell

152   proteins of the best-expressing transformants (Supplemental Figure 1) were analyzed

153   on the same immunoblot using an antibody against GFP (Figure 1C).

154

155   With respect to cytosolic-localized constructs, we found that expression of the sensor

156   driven by the pAR promoter, with omission of the C-terminal 3xHA tag, was ~2-fold

157   higher than the *PSAD* promoter-driven construct (Figure 1C). Furthermore, unfused

158   roGFP2 was expressed at about the same level as the full sensor (Figure 1C). For

159   targeting to the mitochondrial matrix, ER, and nucleus we employed HSP70C (heat

160   shock protein 70C) and BiP2 targeting sequences as well as an SV40 (Simian Virus

161   40) nuclear localization signal. For each construct, we found single protein bands in

6

162 immunoblots and correct sensor localization as confirmed by confocal fluorescence

163 microscopy (Figures 1C and 1D). For targeting to the chloroplast stroma, we tested

164 three different transit peptides derived from USPA (universal stress protein A),

165 HSP70B, and CDJ1 (chloroplast DnaJ homolog). A double band was observed in all

166 USPA transformants and some GFP fluorescence was observed in the cytosol

167 (Figures 1C and 1D; Supplemental Figure 1). We therefore reasoned that the USPA

168 transit peptide was not efficiently driving chloroplast import. Likewise, as judged from

169 the protein double band and residual GFP fluorescence in the cytosol, the HSP70B

170 transit peptide was also unable to efficiently drive sensor import into chloroplasts

171 (Figures 1C and 1D). In contrast, using the CDJ1 transit peptide, we observed a

172 single protein band in Western blots and an exclusive chloroplast localization judged

173 by fluorescence microscopy (Figures 1C and 1D). We also wanted to target the

174 sensor to the thylakoid lumen and for this created level 0 parts encoding the bipartite

175 signaling sequences from the PSAN and PSBO proteins, which are nuclear-encoded

176 subunits of photosystem I and II, respectively. PSAN uses the TAT pathway for the

177 import of folded proteins, while PSBO uses the Sec pathway for the import of

178 unfolded proteins (Albiniak et al., 2012). Immunological detection of the sensor in the

179 best-expressing PSAN and PSBO transformants showed that the sensor

180 accumulated only to about half of the levels detected in the pAR transformant.

181 Moreover, in PSAN transformants, multiple protein bands were detected that

182 migrated with larger apparent mass than expected for the mature protein (Figure 1C,

183 Supplemental Figure 1). GFP fluorescence was detectable all over the chloroplast

184 and even in the cytosol (Figure 1D), indicating incomplete import of the sensor into

185 both, chloroplast and thylakoid lumen by the PSAN bipartite targeting sequence. In

186 contrast, in PSBO transformants only one major protein band migrating with the

187 expected mass was detected and GFP fluorescence was restricted to the thylakoid

188 lumen, indicating full functionality of the PSBO bipartite targeting signal (Figures 1C

189 and 1D, Supplemental Figure 1).

190 **RoGFP2-Tsa2ΔC$_R$ functions as an ultra-sensitive H$_2$O$_2$ sensor in**

191 **Chlamydomonas**

192 We first tested whether we could detect the cytosolic roGFP2-Tsa2ΔC$_R$ sensor and

193 monitor its oxidation by exogenously added H$_2$O$_2$ in real time. To this end, we took

7

194   cells of the best-expressing pPSAD transformant. Cells were concentrated by

195   centrifugation in a 96 well microtiter plate and GFP fluorescence was monitored after

196   adding 0, 0.1, 0.5, and 1 mM H_2O_2 in a fluorescence plate reader. Note that these

197   H_2O_2 concentrations are initial exogenous concentrations; in HeLa cells, the resulting

198   intracellular H_2O_2 concentrations have been estimated to be several hundred-fold

199   lower (Huang and Sikes, 2014). As shown in Figure 2A, we could indeed detect

200   sensor oxidation in a dose-dependent manner, but the signal was very noisy. In

201   contrast, a clear H_2O_2 concentration-dependent sensor response was observed in

202   the pAR transformant (Figure 2B), presumably because sensor expression was more

203   than two-fold higher than in the pPSAD transformant. The cytosolic roGFP2-Tsa2ΔC_R

204   sensor was ~20% oxidized at steady state at the beginning of our assays. Upon H_2O_2

205   addition, we observed a rapid probe oxidation, which slowly recovered over a period

206   of ~80 min, presumably in a GSH/glutaredoxin-dependent manner as previously

207   shown in yeast (Morgan et al, 2016). The unfused cytosolic roGFP2 was completely

208   unresponsive to H_2O_2 (Figure 2C), confirming the requirement of the Tsa2 moiety to

209   couple roGFP2 oxidation with changes in H_2O_2 availability. Interestingly, the kinetics

210   of roGFP2-Tsa2ΔC_R oxidation and reduction were very similar to those observed in

211   yeast (Morgan et al., 2016). This included a reduction of sensor oxidation over time in

212   the untreated samples, which in yeast was shown to be caused by cell-dependent

213   oxygen consumption from the assay buffer. This observation strongly suggests that

214   roGFP2-Tsa2ΔC_R functions as an ultra-sensitive sensor in Chlamydomonas and is

215   capable of sensing and responding to changes in basal cytosolic H_2O_2 levels, as it

216   does in yeast.

217

218   Having confirmed the feasibility of measurements with cytosolic roGFP2-Tsa2ΔC_R,

219   we next tested the response to exogenously added H_2O_2 of the sensors targeted to

220   the five additional cellular compartments. Under steady state conditions, stromal and

221   mitochondrial sensors were more oxidized than those in the cytosol and nucleus

222   (Figures 2B, D, F, G). However, as for the cytosolic sensor, in response to

223   exogenous H_2O_2 we observed a rapid dose-dependent oxidation followed by slow

224   reduction, for sensors targeted to the chloroplast stroma, thylakoid lumen,

225   mitochondrial matrix and the nucleus (Figure 2D–G). Measurements were not

226   possible in the ER as the sensor was found to be fully oxidized at steady state

8

227 (Figure 2H). Signal noise inversely correlated with the expression level of the sensor:

228 the highest noise was detected for the thylakoid lumen sensor, which was expressed

229 at about two-fold lower levels than the sensors in the stroma and nucleus, which

230 showed least noise (Figures 1C and 2D, E, G). The nuclear, stromal, and thylakoid

231 lumen-localized sensors were reduced at faster rates than their counterparts in the

232 cytosol and mitochondrial matrix (Figures 2B, D-G). Overall, the cytosolic sensor

233 exhibited the highest sensitivity to exogenously added H_2O_2 and the nuclear sensor

234 the lowest, as judged from their responsiveness to the lowest H_2O_2 concentration

235 employed (0.1 mM) (Figure 2B, G). This result may indicate that H_2O_2 scavenging

236 enzymes in the cytosol limit the diffusion of exogenous H_2O_2 to the intracellular

237 organelles

238 RoGFP2-Tsa2ΔC$_R$ reveals the formation of light-dependent subcellular H_2O_2

239 gradients

240 Having established Chlamydomonas lines with sensors in different subcellular

241 compartments, we asked whether we could detect changes in H_2O_2 levels under

242 challenging environmental conditions. We first tested whether exposing cells to high

243 light resulted in increased H_2O_2 levels in the chloroplast stroma and whether H_2O_2

244 could diffuse into other subcellular compartments. The fluorescence assay used so

245 far allowed monitoring the sensor oxidation state in real time. However, as we had no

246 way to illuminate cells in our plate reader assay, we turned to a 'redox trapping'

247 approach. We adopted a protocol from yeast that allows for a rapid 'trapping' of the

248 sensor oxidation state with the membrane permeable alkylating agent N-

249 ethylmaleimide (NEM) (Morgan et al., 2016). NEM irreversibly alkylates free thiol

250 groups, thus preventing further probe oxidation or reduction. We grew transformants

251 expressing the sensor in the cytosol, nucleus, matrix, stroma, and thylakoid lumen

252 under low light of 30 μmol photons m^{-2} s^{-1} to mid-log phase. Cultures were then kept

253 at low light or exposed to 1000 μmol photons m^{-2} s^{-1} in the absence or presence of 3-

254 (3,4-dichlorophenyl)-1,1-dimethylurea (DCMU) to block PET. Cells were harvested

255 before and during the time course of the treatment and the oxidation state of the

256 sensor was measured by plate reader after NEM-trapping. Upon shifting cells into

257 high light, H_2O_2 levels in the stroma increased rapidly within minutes and remained at

258 higher levels when compared with cells kept under low-light during the 20-min time

9

259   course (Figure 3A). The cytosolic probe also responded rapidly, although probe

260   oxidation appeared to recover after 20 min. With slower kinetics, we also observed a

261   slight, non-significant trend towards higher H_2O_2 levels in high light in the

262   mitochondrial matrix, while no increase could be detected in the nucleus (Figures 3C

263   and 3D). The increase in H_2O_2 levels in all tested compartments was abolished when

264   cells were exposed to high light in the presence of DCMU, indicating that H_2O_2 in

265   high light was produced by PET. Because of its low signal to noise ratio (Figure 2E),

266   we were unable to monitor the response of the thylakoid lumen sensor in this assay.

267

268   That we could not detect any increase of H_2O_2 levels in the nucleus of

269   Chlamydomonas cells exposed to high light appeared surprising because such an

270   increase was previously observed in *Nicotiana benthamiana* epidermal cells exposed

271   to 1000 µmol photons m^{-2} s^{-1} (Exposito-Rodriguez et al., 2017). We therefore

272   repeated our experiment at higher light intensities of 1500 µmol photons m^{-2} s^{-1} for 30

273   min but were still not able to detect an increase of H_2O_2 levels in the nucleus (Figure

274   3E).

275

276   Metronidazole and paraquat, also known as methyl viologen, both facilitate the

277   Mehler reaction in intact cells, i.e., the transfer of electrons from PSI to oxygen to

278   produce superoxide, which is converted to H_2O_2 by superoxide dismutase (Mehler,

279   1951; Asada, 2000). While paraquat is directly reduced by PSI, metronidazole is

280   reduced by ferredoxin (Schmidt et al., 1977). Paraquat is active at much lower

281   concentrations than metronidazole. We employed both drugs to test, whether the

282   enhanced rates of H_2O_2 produced in their presence even under low light intensities

283   can be detected in the nucleus. As shown in Figure 3E, this was indeed the case. We

284   also monitored H_2O_2 production upon metronidazole treatment in the stroma, cytosol,

285   and matrix and found H_2O_2 levels to increase in all these subcompartments. In all

286   cases, DCMU reduced the accumulation of H_2O_2 but did not abolish it, most likely

287   because plastoquinone reduction here occurs from starch breakdown via the Ndh2

288   protein mediating so-called pseudo-linear electron transport (Bulté et al., 1990; Mus

289   et al., 2005; Desplats et al., 2009). This was also observed in Arabidopsis seedlings

290   treated with paraquat and DCMU in the light (Ugalde et al., 2020).

291

10

292　In summary, our data show a rapid, PET-dependent increase in H_2O_2 levels in the
293　chloroplast stroma. While H_2O_2 levels produced by metronidazole or paraquat feeding
294　were so high that H_2O_2 readily diffused into all other subcompartments, H_2O_2
295　production under high light was of sufficient magnitude to increase cytosolic H_2O_2 but
296　did not impact significantly upon H_2O_2 levels in the mitochondrial matrix or nucleus.
297　Thus, these results are consistent with our exogenous H_2O_2 application experiments,
298　suggesting that the cytosol acts as an effective barrier, which limits the intracellular
299　diffusion of H_2O_2 concentrations typically produced under physiological conditions.

300　**Heat stress derived H_2O_2 is independent of photosynthetic electron transport**

301　We chose heat stress as a second environmental challenge. To test whether H_2O_2
302　levels within Chlamydomonas cells changed under heat stress, we employed the cell
303　line expressing the H_2O_2 sensor in the cytosol, as this sensor exhibited the highest
304　signal-to-noise ratio (Figure 2B). To allow us to monitor real-time changes in cytosolic
305　H_2O_2 during heat stress, we developed an experimental setup in which cells were
306　cultivated under agitation and continuously circulated to a quartz cuvette inserted into
307　a spectrofluorometer via connected tubing and a peristaltic pump. The culture flask,
308　equipped with a temperature sensor, was kept on a platform well above the water
309　surface of a 40°C water bath, placed into the water bath 20 min after the
310　fluorescence recording had started, and placed back onto the platform another 30
311　min later for recovery. Interestingly, sensor oxidation and thus H_2O_2 production
312　occurred immediately after the temperature had increased and immediately declined
313　when the temperature had dropped again (Figure 4A). When the initial starting
314　temperature was reached after 30 min of recovery, probe oxidation had not fully
315　recovered, yet. To verify that the change in fluorescent light emission under heat
316　stress was not caused by a heat-induced conformational change of the sensor, we
317　trapped the sensor with NEM in steady state as well as in the fully oxidized and fully
318　reduced states and recorded fluorescent light emission after excitation at 405 and
319　488 nm at 25°C, 30°C, 35°C, 40°C, and 45°C. As shown in Supplemental Figure 2,
320　we observed no change in fluorescence emission intensities, indicating that in this
321　temperature range the sensor is stable and that the changes in fluorescence
322　emission under heat stress are indeed caused by changes in roGFP2 oxidation as a
323　result of changes in cellular H_2O_2 levels.

11

324

325   As a further test of our observations, we used the same setup employed for the high

326   light experiments (Figure 2). Specifically, samples were taken from a culture

327   expressing the cytosolic sensor before shifting the temperature from 23°C to 40°C,

328   when the culture was exposed to 40°C for 30 min, and 30 min after shifting the

329   culture back to 23°C. The redox state of the sensor was measured after trapping with

330   NEM. As shown in Figure 4B, we could confirm that heat stress leads to a transient

331   increase in cytosolic H_2O_2 levels, which was abolished when the temperature

332   dropped again. As the increase in H_2O_2 levels was the same in the presence of

333   DCMU (Figure 4B), we can conclude that H_2O_2 produced during heat stress does not

334   derive from PET.

335

336

337   **Discussion**

338   **RoGFP2-Tsa2ΔC$_R$ is a novel sensor for the detection of H$_2$O$_2$ in five**
339   **Chlamydomonas compartments**

340   Here we report on the development of Chlamydomonas lines expressing the ultra-
341   sensitive, genetically encoded H$_2$O$_2$ sensor roGFP2-Tsa2ΔC$_R$ (Morgan et al., 2016)
342   in five different subcellular compartments (cytosol, nucleus mitochondrial matrix,
343   chloroplast stroma, and thylakoid lumen). The establishment of the sensor in
344   Chlamydomonas was facilitated by using the Modular Cloning (MoClo) technology
345   (Weber et al., 2011) and the recently generated Chlamydomonas MoClo kit (Crozet
346   et al., 2018). The interchangeability of individual parts and the ability to assemble
347   them in a single reaction, combined with the short generation time of
348   Chlamydomonas, enabled iterative cycles of construct production and testing in a
349   very short time frame. This way, problems encountered with insufficient promoter
350   activity or inefficient targeting to the chloroplast and thylakoid lumen could be rapidly
351   solved.

352

353   We demonstrate the suitability of roGFP2-Tsa2ΔC$_R$ to monitor intracellular H$_2$O$_2$
354   levels in Chlamydomonas with three different experimental setups, each having
355   inherent advantages and disadvantages. First, we developed an assay using
356   microtiter plates in a plate reader (Figure 2). The advantage here is that changes in
357   H$_2$O$_2$ levels can be monitored in real-time and with high throughput. The
358   disadvantage of this assay is that cells need to be concentrated by centrifugation and
359   we have no way to use this approach for the monitoring of responses to changes in
360   light intensity. Second, we continuously circulated cells between culture flask and a
361   cuvette in a spectrofluorometer (Figure 4A). The advantage of this setup is that
362   changes in H$_2$O$_2$ levels can be monitored in real-time under physiological conditions
363   (if the dark period in the cuvette is not a problem). The disadvantage is the low
364   throughput. Third, we trapped the sensor oxidation state with NEM (Figures 3 and
365   4B). The advantage here is that measurements are under fully physiological
366   conditions at medium throughput. The disadvantage is that H$_2$O$_2$ levels are not
367   monitored in real time and therefore rapid H$_2$O$_2$ dynamics may be missed. The

13

368 decision of which setup to employ needs to be made depending on the specific
369 biological question asked.

Properties of the roGFP2-Tsa2ΔC$_R$ sensor in Chlamydomonas cells

371 Overall, the kinetics of oxidation and reduction of roGFP2-Tsa2ΔC$_R$ after the
372 exogenous addition of H_2O_2 were very similar to those observed for this sensor in
373 yeast (Morgan et al., 2016) and for the roGFP2-Orp1 sensor in Arabidopsis seedings
374 (Ugalde et al., 2020). Consistent with previous observations in yeast, we observed
375 that cytosolic roGFP2-Tsa2ΔC$_R$ was more than 20% oxidized at steady state and that
376 the oxidation of the untreated control sample decreased over time. In yeast, this
377 decrease in sensor oxidation was shown to be caused by decreasing oxygen levels
378 in the assay buffer (Morgan et al, 2016). Thus, our observations indicate that, as in
379 yeast, roGFP2-Tsa2ΔC$_R$ functions as an ultra-sensitive H_2O_2 sensor in
380 Chlamydomonas that enables the monitoring of 'basal' cellular H_2O_2 levels. Although
381 difficult to compare between organisms and experimental setups, we also note that
382 whilst 0.1 mM of exogenously added H_2O_2 induced a strong roGFP2-Tsa2ΔC$_R$
383 response in Chlamydomonas, 2 mM H_2O_2 was required to elicit a roGFP2-Orp1
384 response in Arabidopsis seedlings (Ugalde et al., 2020).

386 RoGFP2-Tsa2ΔC$_R$ targeted to the ER was fully oxidized (Figure 2H). Full oxidation
387 was also observed for an unfused roGFP2 targeted to the ER of tobacco leaf cells
388 (Meyer et al., 2007) and for HyPer targeted to the ER in mammalian cells (Mehmeti
389 et al., 2012). This is almost certainly due to the oxidative milieu in the ER lumen
390 rather than to high ER lumenal H_2O_2 concentrations (Mehmeti et al., 2012).
391 Specifically, the ER maintains an active disulfide generating machinery and a
392 relatively oxidized glutathione pool (in the absence of glutaredoxins) that does not
393 allow sensor reduction (Schwarzlander et al., 2016). Hence, in this compartment
394 disulfide bond formation is largely favored over disulfide reduction.

396 Cytosolic roGFP2 alone was insensitive to exogenously added H_2O_2 and found to be
397 constantly in a highly reduced state (Figure 2C). RoGFP2 has been shown to be in
398 equilibrium with the 2GSH/GSSG redox couple, which is catalyzed by enzymatically
399 active glutaredoxin (Gutscher et al., 2008; Marty et al., 2009; Morgan et al., 2013).

14

400   This points to a large excess of GSH over GSSG in the Chlamydomonas cytosol, as

401   is the case for the cytosol of a wide variety of other cell types (Schwarzlander et al.,

402   2016).

403

404   HyPer has been reported to be susceptible to gene silencing beyond the cotyledon

405   stage in Arabidopsis (Exposito-Rodriguez et al., 2013). Although silencing can be

406   circumvented, for example by transient expression in *Nicotiana benthamiana* abaxial

407   epidermal cells (Exposito-Rodriguez et al., 2017), this is not ideal. We found no

408   silencing of our roGFP2-Tsa2ΔC_R constructs over a period of 1–2 years in

409   Chlamydomonas. However, although we employed all 'tricks' for high-level transgene

410   expression, which included using the strongest promoter currently available

411   (*HSP70A-RBCS2*), a codon-optimized ORF containing the three *RBCS2* introns, the

412   *RPL23* terminator, and the UVM4 expression strain (Schroda, 2019), sensor

413   expression was only just sufficient to achieve a good signal-to-noise ratio in most

414   compartments. When expression levels were reduced by about half, i.e. when the

415   *PSAD* promoter was used instead of the *AR* promoter, or when the sensor was

416   targeted to the thylakoid lumen, the signal became too noisy for reliable

417   measurements. Hence, for future applications of this sensor, care must be taken that

418   expression levels in the chosen Chlamydomonas strain are sufficiently high.

419   **H_2O_2 produced by PET in the stroma under physiological conditions readily**

420   **diffuses into the cytosol but not to other subcellular compartments**

421   Our observations demonstrated the suitability of roGFP2-Tsa2ΔC_R to monitor H_2O_2

422   levels under physiologically relevant conditions. For example, under high light

423   intensities (1000 μmol photons m^{-2} s^{-1}) we observed a rapid, PET-dependent

424   increase in stromal H_2O_2 levels, together with a concomitant increase in cytosolic

425   H_2O_2. Changes in H_2O_2 in the mitochondrial matrix were barely detectable and no

426   change was observed in the nucleus. We also could not detect an increase in H_2O_2

427   levels in the nucleus, even when we increased the light intensity to 1500 μmol

428   photons m^{-2} s^{-1} (Figures 3D, 3E). But we could detect H_2O_2 in the nucleus and

429   mitochondria of cells supplemented with paraquat and/or metronidazole at low light

430   intensities (Figure 3E). Thus, our findings partially corroborate earlier studies, which

431   reported leakage of PET-dependent H_2O_2 from the chloroplast into other

15

432   compartments (Mubarakshina et al., 2010; Caplan et al., 2015; Exposito-Rodriguez et

433   al., 2017; Ugalde et al., 2020). However, our results also indicate that the H_2O_2

434   scavenging capacity of the cytosol is sufficiently high to quench the comparably low

435   H_2O_2 concentrations originating from high light exposure, which effectively limits H_2O_2

436   diffusion into other subcellular compartments. In contrast, the cytosolic H_2O_2

437   scavenging capacity appears to become overwhelmed by the high H_2O_2

438   concentrations produced in the presence of metronidazole or paraquat (or

439   exogenously added H_2O_2) and therefore H_2O_2 is not prevented from reaching other

440   subcellular compartments. In summary, our results strongly support the conclusion

441   that cellular H_2O_2 scavenging enzymes limit the intracellular diffusion of H_2O_2 thereby

442   leading to the establishment of steep intracellular H_2O_2 concentration gradients. This

443   interpretation would be in line with the observation that efficient transfer of H_2O_2 from

444   chloroplasts to the nucleus in plant cells required that the two compartments are in

445   close proximity. This is possible because of the mobility of chloroplasts in higher

446   plants cells and appears unlikely for the architecture of Chlamydomonas cells with a

447   single, large chloroplast.

H_2O_2 is produced rapidly under heat stress and does not derive from PET

449   We found H_2O_2 levels to increase rapidly and transiently during heat stress (Figure

450   4). Rapid accumulation of H_2O_2 has been reported previously in tobacco seedlings,

451   spinach leaves, or Arabidopsis and tobacco cell cultures when exposed to heat

452   stress and therefore appears to be a conserved response in plant cells (Foyer et al.,

453   1997; Vacca et al., 2004; Volkov et al., 2006; Gómez et al., 2008). In

454   Chlamydomonas, H_2O_2 levels closely paralleled the temperature change in the

455   culture and therefore H_2O_2 appears to be derived from a constitutive temperature-

456   dependent cellular process (Figure 4A). As the increase in H_2O_2 levels was also

457   observed in the presence of DCMU, it cannot derive from PET. However, there are

458   many alternative production sites for H_2O_2 in plant cells that could be temperature

459   controlled, such as the mitochondrial respiratory chain, limited substrate oxidases

460   (with glycolate, xanthin, urate, sulfite, mono- and polyamines as substrates), type III

461   peroxidases, or NADH oxidases in the plasma membrane (Cheeseman, 2007; Sun

462   and Guo, 2016). Photorespiration is an unlikely source for H_2O_2 in Chlamydomonas,

463   as it depends on input of electrons from PET and Chlamydomonas has a glycolate

16

464   dehydrogenase that does not produce H_2O_2, rather than a glycolate oxidase (Kern et
465   al., 2020).

466

467   Despite the rapid increase in H_2O_2 levels upon heat stress, Chlamydomonas cells
468   induced the expression of scavenging enzymes such as superoxide dismutases,
469   catalase, peroxiredoxins, or dehydroascorbate reductase only between 3 h and 24 h
470   after the temperature shift (Mühlhaus et al., 2011; Hemme et al., 2014; Schroda et
471   al., 2015). This indicates that the increased levels of H_2O_2 upon heat exposure are
472   not detrimental to the cells during the first hours at elevated temperatures and might
473   play a role in signaling.

474

475   In summary, we report on the generation of constructs enabling the expression of the
476   ultra-sensitive H_2O_2 probe, roGFP2-Tsa2ΔC_R, in five different subcellular
477   compartments in Chlamydomonas. We show that these sensors respond readily to
478   both exogenously added and endogenously produced H_2O_2 and reveal that, by
479   following the response of sensors targeted to multiple subcellular compartments, the
480   existence of intracellular H_2O_2 gradients can be inferred. We anticipate that the future
481   application of these sensors will allow exciting new insights into subcellular H_2O_2
482   homeostasis and dynamics.

483

17

484

18

485   **Methods**

486   **Strains and Culture Conditions**

487   *Chlamydomonas reinhardtii* UVM4 cells (Neupert et al., 2009) were grown in Tris-
488   Acetate-Phosphate (TAP) medium (Kropat et al., 2011) on a rotatory shaker at a
489   constant light intensity of ~40 µmol photons m^{-2} s^{-1}. For high-light exposure, cells
490   were grown to ~$1x10^6$ cells/ml, transferred to an open 1-L beaker, placed on an
491   orbital shaker, and exposed to 1000 or 1500 µmol photons m^{-2} s^{-1} provided by CF
492   Grow® (CXB3590-X4). Transformation was done with the glass beads method
493   (Kindle, 1990) as described previously (Hammel et al., 2020) with constructs
494   linearized with NotI. Transformants were selected on 100 µg ml^{-1} spectinomycin.

495   **Cloning of sensor and signal peptide coding sequences**

496   The roGFP2-Tsa2ΔC$_R$ sequence (Morgan et al., 2016) was reverse translated using
497   the most-preferred Chlamydomonas codons and equipped with the three
498   Chlamydomonas *RBCS2* introns as suggested previously for foreign genes (Schroda,
499   2019), but using the native flanking sites of these introns (CAA/In1/GAT,
500   ACG/In2/GCT, and TGC/In3/CTG). An AAG Lys codon was converted into the
501   suboptimal AAA Lys codon to eliminate a GAAGAC BpiI recognition site. The
502   sequence was flanked with BsaI cleavage sites such that upon BsaI digestion a
503   2132-bp fragment with AATG and TTCG overhangs is generated for the B3/4 position
504   of level 0 parts according to the Modular Cloning (MoClo) syntax for plant genes
505   (Weber et al., 2011; Patron et al., 2015) (Figure 1A). Synthesis and cloning into the
506   pUC57 vector was done by GeneCust (Luxembourg), giving rise to pMBS419. The
507   latter   was   used   as   template   for   PCR   with   primers   5'-
508   TTGAAGACATAATGGCCAGCGAGTTCAGC-3'   and   5'-
509   TTGAAGACTCCGAACCCTTGTACAGCTCGTCCATGCC-3'   to amplify a 898-bp
510   fragment containing only the roGFP2 coding sequence with the first *RBCS2* intron
511   (BpiI recognition sites are underlined). The PCR product was combined with
512   destination vector pAGM1287 (Weber et al., 2011), digested with BpiI and assembled
513   by ligation into level 0 construct pMBS467. The level 0 part encoding the HSP70B
514   chloroplast transit peptide was generated via PCR on plasmid pMBS197 using
515   primers   5'-TTGAAGACAACCATGCCGGTTCAGCAGATGAC-3'   and   5'-

19

516   TT<u>GAAGAC</u>AACATTGCCTGAAGGAACAATTCAAATG-3'. This plasmid harbors the

517   coding sequence for the HSP70B transit peptide with an intron, in which a BsaI

518   recognition site had been eliminated. The resulting 251-bp product and plasmid

519   pAGM1276 (Weber et al., 2011) were digested with BpiI and ligated to yield

520   pMBS639. The level 0 part for the chloroplast transit peptide of CDJ1 was produced

521   accordingly   by   PCR   using   primers   5'-

522   TT<u>GAAGAC</u>AACCATGCTCGCAAACCTTCGTAG-3'   and   5'-

523   TT<u>GAAGAC</u>AACATtCCGTCGGCCCGCACAACCAC-3' on genomic DNA, generating

524   a 166-pb product and giving rise to pMBS640. The same procedure was used to

525   produce level 0 parts for bipartite transit peptides for stroma and thylakoid lumen of

526   PSAN   and   PSBO,   using   primers   5'-

527   AA<u>GAAGAC</u>CACCATGGCCATCTCTGCTCGCTC-3'   and   5'-

528   TT<u>GAAGAC</u>GGCATTCCGGCGTTGGCGACGGGGGC-3',   and   primers   5'-

529   TT<u>GAAGAC</u>AACCATGGCCCTCCGCGCTGCCCA-3'   and   5'-

530   TT<u>GAAGAC</u>AACATTGCgAGGGCGTTGGCCGACTGCGA-3'   to   generate   PCR

531   products of 508 bp and 470 bp, giving rise to pMBS298 (PSAN) and pMBS641

532   (PSBO), respectively. All PCRs were done with Q5 High-Fidelity Polymerase (NEB)

533   following the manufacturer's instructions. Correct cloning was verified by Sanger

534   sequencing. These newly constructed level 0 parts were then complemented with

535   level 0 parts (pCM) from the Chlamydomonas MoClo toolkit (Crozet et al., 2018) to fill

536   the respective positions in level 1 modules as follows: A1-B1 – pCM0-015 (*HSP70A-*

537   *RBCS2* promoter + 5'UTR) or pCM0-010 (*PSAD* promoter + 5'UTR); A1-B2 – pCM0-

538   020 (*HSP70A-RBCS2* promoter + 5'UTR) or pCM0-016 (*PSAD* promoter + 5'UTR);

539   B2 – pCM0-053 (USPA chloroplast transit peptide), pMBS639 (HSP70B chloroplast

540   transit peptide), pMBS640 (CDJ1 chloroplast transit peptide), pMBS298 (PSAN

541   thylakoid lumen targeting peptide), pMBS641 (PSBO thylakoid lumen targeting

542   peptide), pCM0-057 (HSP70C mitochondrial transit peptide), or pCM0-056 (BIP ER

543   targeting signal); B3/4 – pMBS419 (roGFP2-Tsa2ΔC$_R$) or pMBS467 (roGFP2); B5 –

544   pCM0-100 (3xHA), pCM0-101 (MultiStop), pCM-111 (BIP ER retention sequence), or

545   pCM-109 (SV40 nuclear localization signal);   B6 – pCM0-119 (*RPL23* 3'UTR). The

546   *HSP70A-RBCS2* fusion promoter used here contains -467 bp of *HSP70A* sequences

547   upstream from the start codon in optimal spacing with respect to the *RBCS2*

548   promoter (Lodha et al., 2008; Strenkert et al., 2013). The respective level 0 parts and

20

549   destination vector pICH47742 (Weber et al., 2011) were combined with BsaI and T4

550   DNA ligase and directionally assembled into the eleven level 1 modules shown in

551   Figure 1B. The level 1 modules were then combined with pCM1-01 (level 1 module

552   with the *aadA* gene conferring resistance to spectinomycin flanked by the *PSAD*

553   promoter and terminator) from the *Chlamydomonas* MoClo kit, with plasmid

554   pICH41744 containing the proper end-linker, and with destination vector pAGM4673

555   (Weber et al., 2011), digested with BpiI, and ligated to yield the eleven level 2

556   devices displayed in Figure 1B. All newly generated level 0 and level 2 plasmids can

557   be ordered from the Chlamydomonas Research Center

558   (https://www.chlamycollection.org/).

Protein analysis by SDS-PAGE

560   Protein extractions, SDS–PAGE, semi-dry blotting and immunodetections were

561   carried out as described previously (Hammel et al., 2020). Antibodies used for

562   immunodetection were mouse anti-HA (Sigma H9658, 1:10,000) and rabbit anti-GFP

563   (Roche, Cat. No. 11814460001). Densitometric band quantifications after

564   immunodetections were done with the FUSIONCapt Advance program (PEQLAB).

RoGFP2 fluorescence recordings

566   RoGFP2 fluorescence was recorded using a CLARIOstar fluorescence plate reader

567   (BMG-Labtech) as described previously for yeast (Morgan et al., 2016) and adopted

568   to Chlamydomonas as follows: Chlamydomonas cells were grown at constant light to

569   a density of ~$3x10^6$ cells/ml. $1x10^7$ cells were used per well and were harvested by

570   centrifugation at 3800 rpm for 2 min at 25°C. Cells were resuspended in 100 mM

571   MES-Tris buffer (pH 7.0) ($5x10^7$ cells/ml) and 200 µl cell suspension were transferred

572   per well of a black, flat-bottomed 96-well imaging plate (BD Falcon 353219). For

573   calibration and later data processing, control samples of fully oxidized and fully

574   reduced sensors were prepared by adding N,N,N′,N′-tetramethylazodicarboxamide

575   (diamide) at a final concentration of 20 mM and DTT at a final concentration of 100

576   mM to cells in two different wells. Further wells to record roGFP2 fluorescence at

577   steady state, at increasing H_2O_2 concentrations, or after different treatments were

578   prepared. Before starting the measurement, the 96-well imaging plate was

579   centrifuged at 30 g for 5 min at 25°C. Chlamydomonas UVM4 recipient cells were

21

580 always included as negative control. The measurement mode of the plate reader was

581 based on the "Fluorescence Intensity" coupled with the "Bottom Optic" option, with a

582 positioning delay of 0.2 sec, 40 flashes per well and the desired number of

583 measurement cycles (about 200 cycles) and time per cycle (about 20 sec). The gain

584 adjustment was set to 80% maximum and an automatic gain adjustment for each

585 wavelength was performed immediately before the measurement. RoGFP2 exhibits

586 two excitation maxima at 400 nm and 475–490 nm when fluorescence emission is

587 monitored at 510 nm. Therefore, it was ensured that the number of multichromatics

588 was set to 2 and that the correct excitation (410 and 480 nm) and emission (510 nm)

589 filters were selected. The measurement was started and increasing H_2O_2 solutions

590 were added after 10 cycles. After the fluorescence measurement was done, MARS

591 Data Analysis software was used to subtract the auto-fluorescence of WT cells. The

592 "blank corrected" values were taken to calculate the degree of sensor oxidation

593 (OxD) using the following equation:

594

595 $OxD\ roGFP2 =$

596 $$\frac{I405_{\text{sample}} \times I488_{\text{red}} - I405_{\text{red}} \times I405_{\text{sample}}}{I405_{\text{sample}} \times I488_{\text{red}} - I405_{\text{sample}} \times I488_{\text{ox}} + I405_{\text{sample}} \times -I405_{red} \times I488_{\text{red}}}$$

597

598 where I is the fluorescence intensity at 510 nm after excitation at either 405 nm or

599 488 nm. The subscripts 'ox', 'red' and 'sample' indicate the fluorescence intensity

600 measured for the fully oxidized and fully reduced controls and the sample,

601 respectively.

602 **NEM-based alkylation for measuring H_2O_2 levels in cell cultures.**

603 The cell number of Chlamydomonas cells grown to 1-3x10^6 cells/ml was determined

604 and the volume to harvest 2.5x10^7 cells was calculated. For rapid 'trapping' of probe

605 oxidation, 50 ml Falcon tubes were preloaded with one fourth of the final volume with

606 100 mM MES-Tris (pH 7.0) buffer containing 40 mM NEM. Chlamydomonas cells

607 were harvested in prefilled Falcon tubes by centrifugation at 3800 rpm for 3 min at

608 room temperature and subsequently resuspended in 500 µl 100 mM MES-Tris (pH

609 7.0) buffer containing 40 mM NEM to a final concentration of 5x10^7 cells/ml. 200 µl

610 (10^7 cells per well) of suspension were transferred to a 96-well plate. For calculating

22

611   the OxD, fully oxidized (diamide) and reduced (DTT) samples were added and probe

612   oxidation was measured following the protocol described above.

613   Continuous monitoring of real-time changes in H_2O_2 during heat stress via

614   connected tubing and a peristaltic pump

615   Chlamydomonas cells (~5×10^6 cells/ml) were cultivated under agitation at a constant

616   light intensity of ~40 μmol photons m^{-2} s^{-1} and continuously circulated to a quartz

617   cuvette inserted into a spectrofluorometer (Jascon FP-8300) via connected tubing

618   and a peristaltic pump (Watson Marlow 101U, flow rate: 1 ml/s). After 20 min, cells

619   were exposed to 40°C for 30 min in a water bath, and shifted back to 23°C for 30

620   min. The ratio of the fluorescent light intensities emitted after excitation at 405 and

621   488 nm was monitored every 30 s. The measurement mode of the

622   spectrofluorometer was based on the "Fixed wavelength measurement" with an

623   excitation bandwidth of 5 nm and an emission bandwidth of 10 nm.

624

625   Confocal microscopy

626   All images were acquired using a Zeiss LSM880 AxioObserver confocal laser

627   scanning microscope equipped with a Zeiss C-Apochromat 40x/1,2 W AutoCorr M27

628   water-immersion objective. Fluorescent signals of green fluorescent protein (GFP)

629   (excitation/emission   488 nm/491-589 nm)   and   chlorophyll   autofluorescence

630   (excitation/emission 633 nm/647-721 nm) were processed using the Zeiss software

631   ZEN 2.3 or ImageJ.

23

632

633   **Supplemental Figure 1.** Screening of transformants expressing the roGFP2 sensor

634   by immunoblotting.

635

636   **Supplemental Figure 2.** Analysis of fluorescence properties of the roGFP2-

637   Tsa2ΔCR sensor at different temperatures.

638

639   **Acknowledgements**

645

646   **Author Contributions**

647   J.N. generated all constructs and performed all experiments. D.S recorded the

648   confocal microscopy images. J.O. helped with setting up the fluorescence recordings.

649   M.S. and B.M. conceived and supervised the project and wrote the article with

650   contributions from all authors.

651

652

653   **Figures and Figure legends**

654
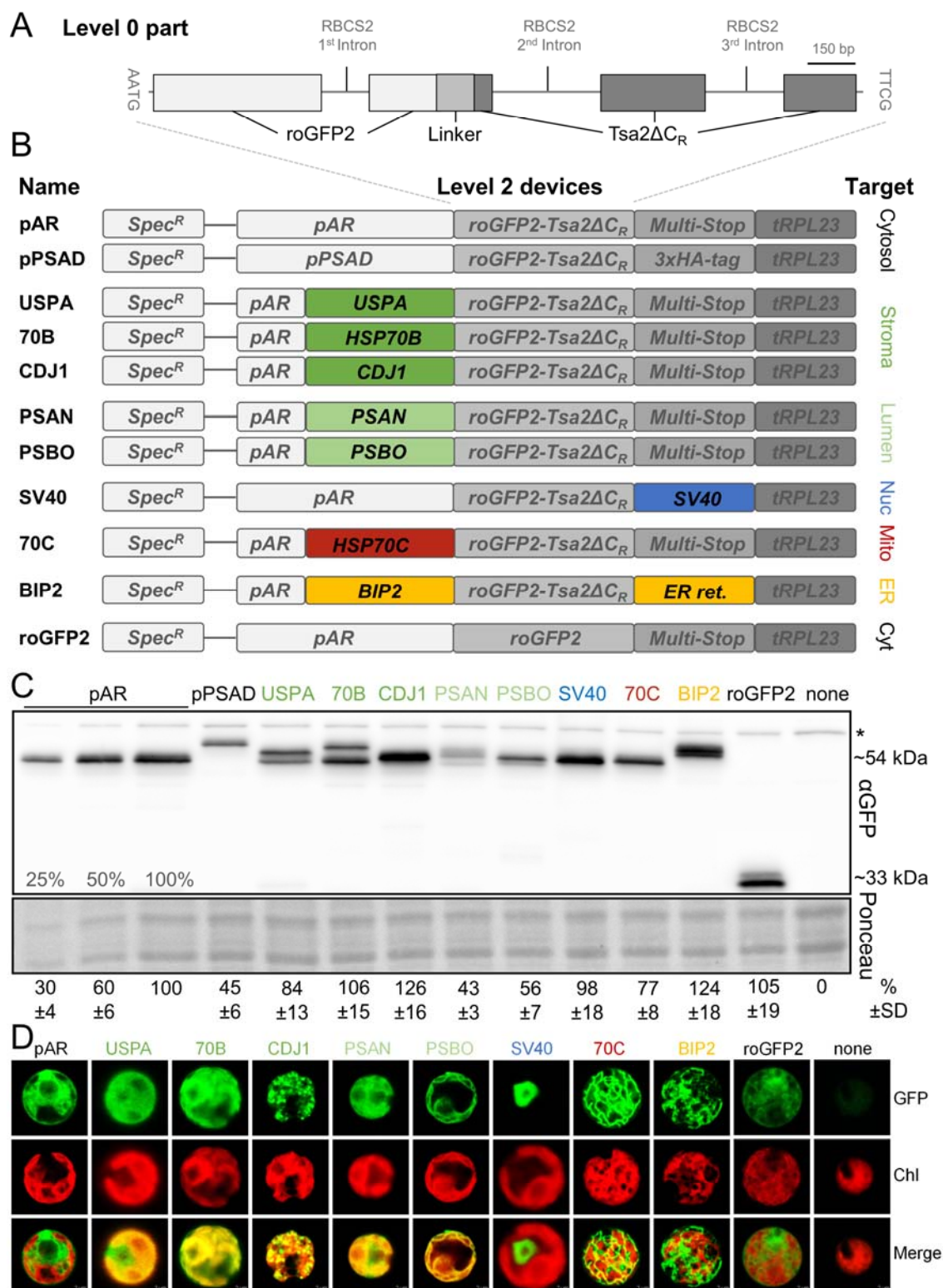
655
656 **Figure 1. Targeting roGFP2 sensors to various compartments of a Chlamydomonas cell**
657 **(A)** Level 0 part of the roGFP2-Tsa2ΔC_R H_2O_2 sensor. The 2132-bp ORF (exons shown as boxes), interrupted by
658 the three RBCS2 introns (thin lines), was synthesized with optimal Chlamydomonas codon usage. RoGFP2 (light
659 grey) is separated from Tsa2ΔCR (dark grey) by a Linker (medium grey).

660 **(B)** Using MoClo, the roGFP2-Tsa2ΔC$_R$ part or only the roGFP2 part were equipped with the *HSP70A-RBCS2*
661 promotor (*pAR*) or the *PSAD* promoter (*pPSAD*) and the *RPL23* terminator (*tRPL23*) as well as various N- and C-
662 terminal targeting sequences to target the sensors to the cytosol (cyt), the stroma, the thylakoid lumen (lumen),
663 the nucleus (nuc), mitochondria (mito), or the endoplasmic reticulum (ER). The resulting level 1 modules were
664 combined with another level 1 module comprising the *aadA* resistance marker flanked by the *PSAD* promoter and
665 terminator (Spec^R) to yield the eleven level 2 devices shown.
666 **(C)** Comparison of roGFP2 expression levels in transformants generated with the level 2 devices shown in (B).
667 The transformants shown represent the ones with highest expression levels among at least 13 transformants
668 screened per construct. Total cell proteins corresponding to 1.5 µg chlorophyll of each transformant and the
669 UVM4 recipient strain (none) were separated by SDS-PAGE and analyzed by immunoblotting using an antibody
670 against GFP. Signals retrieved from three independent experiments were quantified and normalized to the signal
671 obtained with the transformant harboring the construct for the expression of cytosolic roGFP2-Tsa2ΔC$_R$ driven by
672 the *HSP70A-RBCS2* promotor (pAR), which was set to 100%. Mean values are given below the panel (± SD). A
673 representative experiment is shown, with Ponceau staining demonstrating equal loading. The asterisk indicates a
674 non-specific cross-reaction with the GFP antibody.
675 **(D)** Confocal microscopy images of individual cells of the best-expressing transformants shown in (C) and the
676 untransformed UVM4 strain (none). Shown are GFP fluorescence, chlorophyll fluorescence (Chl) and both signals
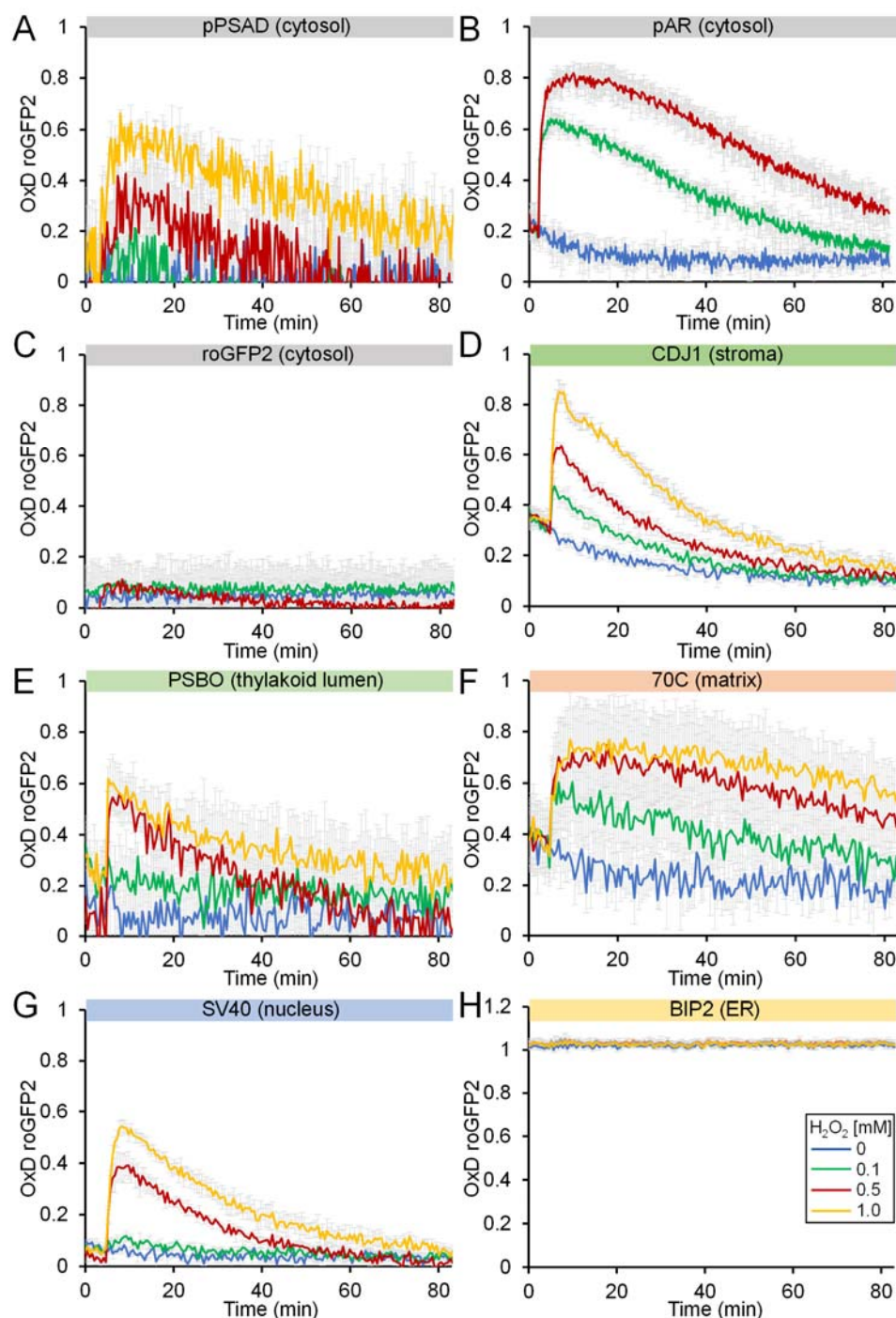677 merged.

26

Figure 2. Real-time monitoring of H$_2$O$_2$ levels in different subcellular compartments under steady-state conditions and after the addition of H$_2$O$_2$

(A-H) Fluorescence measurement of roGFP2-Tsa2ΔC$_R$ and roGFP2 in transformant cells shown in Figure 1C and 1D under steady-state conditions (no H$_2$O$_2$ added, blue) and after the addition of H$_2$O$_2$ at concentrations of 0.1 mM (green), 0.5 mM (red), and 1 mM (yellow). Values were calculated relative to those obtained for fully reduced (0) and fully oxidized (1) sensors. Shown are means of three independent experiments, error bars represent standard deviations.
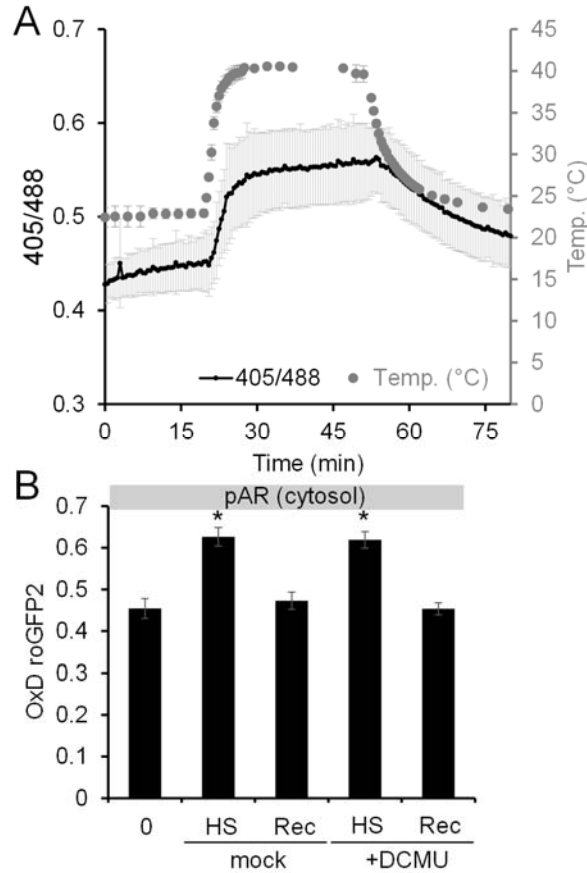
27

Figure 3. Monitoring H_2O_2 levels in different subcellular compartments under high-light exposure and the application of metronidazole and paraquat

Chlamydomonas transformant cells, expressing roGFP2-Tsa2ΔC$_R$ in the stroma **(A)**, cytosol **(B)**, mitochondrial matrix **(C)**, and nucleus **(D)** were kept in low light of 30 µmol photons m^{-2} s^{-1} (blue) or exposed to high light of 1000 µmol photons m^{-2} s^{-1} in the absence (yellow) or presence (red) of 10 µM DCMU. The oxidation state of the sensor was trapped by the addition of NEM and roGFP2 fluorescence was measured in a plate reader. Shown are mean values from three independent experiments, error bars represent standard deviations. Asterisks indicate significant differences with respect to the low light control (t-Test, $p < 0.01$). **(E)** Transformant cells expressing roGFP2-Tsa2ΔC$_R$ in the compartments indicated were grown in low light of 30 µmol photons m^{-2} s^{-1} (0) and exposed to 1500 m^{-2} s^{-1} for 30 min, or kept at low light for 30 min in the presence of 2 mM metronidazol (M) or 1 µM paraquat (P), both in the absence or presence of 10 µM DCMU (D). The oxidation state of the sensor was trapped by the addition of NEM and roGFP2 fluorescence was measured in a plate reader. Error bars represent standard deviations from three independent experiments. Asterisks indicate significant differences with respect to the low light control (t-Test, $p < 0.05$).

28

715

716
717
718
719 **Figure 4. Monitoring H$_2$O$_2$ levels in the cytosol during heat stress and recovery**
720 **(A)** Chlamydomonas cells expressing roGFP2-Tsa2ΔC$_R$ in the cytosol were grown in low light of 30 µmol photons
721 m^{-2} s^{-1} for 20 min, exposed to 40°C for 30 min, and shifted back to 23°C for 30 min. The ratio of the fluorescence
722 light emitted after excitation at 405 and 488 nm, respectively, was monitored in real time using a
723 spectrofluorometer (black line). The temperature in the culture was monitored in parallel (grey circles). Shown are
724 mean values from three independent experiments, error bars represent standard deviations
725 **(B)** Transformant cells expressing roGFP2-Tsa2ΔC$_R$ in the cytosol were grown in low light of 30 µmol photons m^{-2}
726 s^{-1} (0) at 23°C, exposed to 40°C for 30 min (HS), and shifted back to 23 for another 30 min (Rec). Cultures were
727 supplied with 10 µM DCMU or only the solvent (mock) before the experiment was started. The oxidation state of
728 the sensor was trapped by the addition of NEM and roGFP2 fluorescence was measured in a plate reader. Error
729 bars represent standard deviations from three independent experiments. Asterisks indicate significant differences
730 with respect to the 23°C control (t-Test, p < 0.001).
731

732

29

733

30

Parsed Citations

Albiniak, A.M., Baglieri, J., and Robinson, C. (2012). Targeting of lumenal proteins across the thylakoid membrane. Journal of experimental botany 63, 1689-1698.
Google Scholar: Author Only Title Only Author and Title

Asada, K. (2000). The water-water cycle as alternative photon and electron sinks. Philos. Trans. R. Soc. Lond. B Biol. Sci. 355, 1419-1431.
Google Scholar: Author Only Title Only Author and Title

Belousov, V.V., Fradkov, A.F., Lukyanov, K.A, Staroverov, D.B., Shakhbazov, K.S., Terskikh, A.V., and Lukyanov, S. (2006). Genetically encoded fluorescent indicator for intracellular hydrogen peroxide. Nature methods 3, 281-286.
Google Scholar: Author Only Title Only Author and Title

Bilan, D.S., and Belousov, V.V. (2018). In Vivo Imaging of Hydrogen Peroxide with HyPer Probes. Antioxidants & redox signaling 29, 569-584.
Google Scholar: Author Only Title Only Author and Title

Bulté, L., Gans, P., Rebéillé, F., and Wollman, F.A. (1990). ATP control on state transitions in vivo in Chlamydomonas reinhardtii. Biochimica et Biophysica Acta (BBA) - Bioenergetics 1020, 72-80.
Google Scholar: Author Only Title Only Author and Title

Caplan, J.L., Kumar, A.S., Park, E., Padmanabhan, M.S., Hoban, K., Modla, S., Czymmek, K., and Dinesh-Kumar, S.P. (2015). Chloroplast Stromules Function during Innate Immunity. Dev. Cell 34, 45-57.
Google Scholar: Author Only Title Only Author and Title

Cheeseman, J. (2007). Hydrogen Peroxide and Plant Stress: A Challenging Relationship. Plant Stress 1.
Google Scholar: Author Only Title Only Author and Title

Crozet, P., Navarro, F.J., Willmund, F., Mehrshahi, P., Bakowski, K., Lauersen, K.J., Perez-Perez, M.E., Auroy, P., Gorchs Rovira, A., Sauret-Gueto, S., Niemeyer, J., Spaniol, B., Theis, J., Trosch, R., Westrich, L.D., Vavitsas, K., Baier, T., Hubner, W., de Carpentier, F., Cassarini, M., Danon, A, Henri, J., Marchand, C.H., de Mia, M., Sarkissian, K., Baulcombe, D.C., Peltier, G., Crespo, J.L., Kruse, O., Jensen, P.E., Schroda, M., Smith, A.G., and Lemaire, S.D. (2018). Birth of a photosynthetic chassis: a MoClo toolkit enabling synthetic biology in the microalga Chlamydomonas reinhardtii. ACS synthetic biology 7, 2074-2086.
Google Scholar: Author Only Title Only Author and Title

Desplats, C., Mus, F., Cuine, S., Billon, E., Cournac, L., and Peltier, G. (2009). Characterization of Nda2, a plastoquinone-reducing type II NAD(P)H dehydrogenase in Chlamydomonas chloroplasts. J. Biol. Chem. 284, 4148-4157.
Google Scholar: Author Only Title Only Author and Title

Exposito-Rodriguez, M., Laissue, P.P., Littlejohn, G.R., Smirnoff, N., and Mullineaux, P.M. (2013). The use of HyPer to examine spatial and temporal changes in H2O2 in high light-exposed plants. Methods Enzymol. 527, 185-201.
Google Scholar: Author Only Title Only Author and Title

Exposito-Rodriguez, M., Laissue, P.P., Yvon-Durocher, G., Smirnoff, N., and Mullineaux, P.M. (2017). Photosynthesis-dependent H2O2 transfer from chloroplasts to nuclei provides a high-light signalling mechanism. Nature communications 8, 49.
Google Scholar: Author Only Title Only Author and Title

Foyer, C.H., and Noctor, G. (2016). Stress-triggered redox signalling: what's in pROSpect? Plant Cell Environ. 39, 951-964.
Google Scholar: Author Only Title Only Author and Title

Foyer, C.H., LopezDelgado, H., Dat, J.F., and Scott, I.M. (1997). Hydrogen peroxide- and glutathione-associated mechanisms of acclimatory stress tolerance and signalling. Physiologia plantarum 100, 241-254.
Google Scholar: Author Only Title Only Author and Title

Gómez, F., Fernández, L., Gergoff, G., Guiamet, J.J., Chaves, A, and Bartoli, C.G. (2008). Heat shock increases mitochondrial H2O2 production and extends postharvest life of spinach leaves. Postharvest. Biol. Technol. 49, 229-234.
Google Scholar: Author Only Title Only Author and Title

Gutscher, M., Sobotta, M.C., Wabnitz, G.H., Ballikaya, S., Meyer, A.J., Samstag, Y., and Dick, T.P. (2009). Proximity-based protein thiol oxidation by H2O2-scavenging peroxidases. J. Biol. Chem. 284, 31532-31540.
Google Scholar: Author Only Title Only Author and Title

Gutscher, M., Pauleau, A.L., Marty, L., Brach, T., Wabnitz, G.H., Samstag, Y., Meyer, A.J., and Dick, T.P. (2008). Real-time imaging of the intracellular glutathione redox potential. Nature methods 5, 553-559.
Google Scholar: Author Only Title Only Author and Title

Hammel, A, Sommer, F., Zimmer, D., Stitt, M., Muhlhaus, T., and Schroda, M. (2020). Overexpression of sedoheptulose-1,7-bisphosphatase enhances photosynthesis in Chlamydomonas reinhardtii and has no effect on the abundance of other Calvin-Benson Cycle enzymes. Frontiers in plant science 11, 868.
Google Scholar: Author Only Title Only Author and Title

Hanson, G.T., Aggeler, R., Oglesbee, D., Cannon, M., Capaldi, R.A, Tsien, R.Y., and Remington, S.J. (2004). Investigating mitochondrial

redox potential with redox-sensitive green fluorescent protein indicators. J. Biol. Chem. 279, 13044-13053.
Google Scholar: Author Only Title Only Author and Title

Hemme, D., Veyel, D., Mühlhaus, T., Sommer, F., Juppner, J., Unger, A.K., Sandmann, M., Fehrle, I., Schönfelder, S., Steup, M., Geimer, S., Kopka, J., Giavalisco, P., and Schroda, M. (2014). Systems-wide analysis of acclimation responses to long-term heat stress and recovery in the photosynthetic model organism Chlamydomonas reinhardtii. Plant Cell 26, 4270-4297.
Google Scholar: Author Only Title Only Author and Title

Huang, B.K., and Sikes, H.D. (2014). Quantifying intracellular hydrogen peroxide perturbations in terms of concentration. Redox Biol 2, 955-962.
Google Scholar: Author Only Title Only Author and Title

Kern, R., Facchinelli, F., Delwiche, C., Weber, A.P.M., Bauwe, H., and Hagemann, M. (2020). Evolution of photorespiratory glycolate oxidase among Archaeplastida. Plants (Basel) 9.
Google Scholar: Author Only Title Only Author and Title

Kindle, K.L. (1990). High-frequency nuclear transformation of Chlamydomonas reinhardtii. Proc. Natl. Acad. Sci. U. S. A. 87, 1228-1232.
Google Scholar: Author Only Title Only Author and Title

Kropat, J., Hong-Hermesdorf, A, Casero, D., Ent, P., Castruita, M., Pellegrini, M., Merchant, S.S., and Malasarn, D. (2011). A revised mineral nutrient supplement increases biomass and growth rate in Chlamydomonas reinhardtii. Plant J. 66, 770-780.
Google Scholar: Author Only Title Only Author and Title

Kwak, J.M., Mori, I.C., Pei, Z.M., Leonhardt, N., Torres, M.A, Dangl, J.L., Bloom, R.E., Bodde, S., Jones, J.D., and Schroeder, J.I. (2003). NADPH oxidase AtrbohD and AtrbohF genes function in ROS-dependent ABA signaling in Arabidopsis. EMBO J. 22, 2623-2633.
Google Scholar: Author Only Title Only Author and Title

Lew, T.T.S., Koman, V.B., Silmore, K.S., Seo, J.S., Gordiichuk, P., Kwak, S.-Y., Park, M., Ang, M.C.-Y., Khong, D.T., Lee, M.A, Chan-Park, M.B., Chua, N.-H., and Strano, M.S. (2020). Real-time detection of wound-induced H2O2 signalling waves in plants with optical nanosensors. Nature Plants 6, 404-415.
Google Scholar: Author Only Title Only Author and Title

Lodha, M., Schulz-Raffelt, M., and Schroda, M. (2008). A new assay for promoter analysis in Chlamydomonas reveals roles for heat shock elements and the TATA box in HSP70A promoter-mediated activation of transgene expression. Eukaryotic cell 7, 172-176.
Google Scholar: Author Only Title Only Author and Title

Marty, L., Siala, W., Schwarzlander, M., Fricker, M.D., Wirtz, M., Sweetlove, L.J., Meyer, Y., Meyer, A.J., Reichheld, J.P., and Hell, R. (2009). The NADPH-dependent thioredoxin system constitutes a functional backup for cytosolic glutathione reductase in Arabidopsis. Proc. Natl. Acad. Sci. U. S. A. 106, 9109-9114.
Google Scholar: Author Only Title Only Author and Title

Mehler, A.H. (1951). Studies on reactions of illuminated chloroplasts. I. Mechanism of the reduction of oxygen and other Hill reagents. Arch. Biochem. Biophys. 33, 65-77.
Google Scholar: Author Only Title Only Author and Title

Mehmeti, I., Lortz, S., and Lenzen, S. (2012). The H2O2-sensitive HyPer protein targeted to the endoplasmic reticulum as a mirror of the oxidizing thiol-disulfide milieu. Free Radic. Biol. Med. 53, 1451-1458.
Google Scholar: Author Only Title Only Author and Title

Meyer, A.J., Brach, T., Marty, L., Kreye, S., Rouhier, N., Jacquot, J.P., and Hell, R. (2007). Redox-sensitive GFP in Arabidopsis thaliana is a quantitative biosensor for the redox potential of the cellular glutathione redox buffer. Plant J. 52, 973-986.
Google Scholar: Author Only Title Only Author and Title

Miller, G., Schlauch, K., Tam, R., Cortes, D., Torres, M.A, Shulaev, V., Dangl, J.L., and Mittler, R. (2009). The plant NADPH oxidase RBOHD mediates rapid systemic signaling in response to diverse stimuli. Science signaling 2, ra45.
Google Scholar: Author Only Title Only Author and Title

Morgan, B., Ezerina, D., Amoako, T.N., Riemer, J., Seedorf, M., and Dick, T.P. (2013). Multiple glutathione disulfide removal pathways mediate cytosolic redox homeostasis. Nat. Chem. Biol. 9, 119-125.
Google Scholar: Author Only Title Only Author and Title

Morgan, B., Van Laer, K., Owusu, T.N., Ezerina, D., Pastor-Flores, D., Amponsah, P.S., Tursch, A, and Dick, T.P. (2016). Real-time monitoring of basal H2O2 levels with peroxiredoxin-based probes. Nat. Chem. Biol. 12, 437-443.
Google Scholar: Author Only Title Only Author and Title

Mubarakshina, M.M., Ivanov, B.N., Naydov, I.A, Hillier, W., Badger, M.R., and Krieger-Liszkay, A. (2010). Production and diffusion of chloroplastic H2O2 and its implication to signalling. Journal of experimental botany 61, 3577-3587.
Google Scholar: Author Only Title Only Author and Title

Mühlhaus, T., Weiss, J., Hemme, D., Sommer, F., and Schroda, M. (2011). Quantitative shotgun proteomics using a uniform 15N-labeled standard to monitor proteome dynamics in time course experiments reveals new insights into the heat stress response of Chlamydomonas reinhardtii. Mol. Cell. Proteomics 10, M110 004739.
Google Scholar: Author Only Title Only Author and Title

Mus, F., Cournac, L., Cardettini, V., Caruana, A, and Peltier, G. (2005). Inhibitor studies on non-photochemical plastoquinone reduction and H2 photoproduction in Chlamydomonas reinhardtii. Biochimica et Biophysica Acta (BBA) - Bioenergetics 1708, 322-332.
Google Scholar: Author Only Title Only Author and Title

Neupert, J., Karcher, D., and Bock, R. (2009). Generation of Chlamydomonas strains that efficiently express nuclear transgenes. Plant J. 57, 1140-1150.
Google Scholar: Author Only Title Only Author and Title

Pak, V.V., Ezerina, D., Lyublinskaya, O.G., Pedre, B., Tyurin-Kuzmin, P.A., Mishina, N.M., Thauvin, M., Young, D., Wahni, K., Martinez Gache, S.A, Demidovich, A.D., Ermakova, Y.G., Maslova, Y.D., Shokhina, A.G., Eroglu, E., Bilan, D.S., Bogeski, I., Michel, T., Vriz, S., Messens, J., and Belousov, V.V. (2020). Ultrasensitive genetically encoded indicator for hydrogen peroxide identifies roles for the oxidant in cell migration and mitochondrial function. Cell Metab 31, 642-653 e646.
Google Scholar: Author Only Title Only Author and Title

Patron, N.J., Orzaez, D., Marillonnet, S., Warzecha, H., Matthewman, C., Youles, M., Raitskin, O., Leveau, A, Farre, G., Rogers, C., Smith, A, Hibberd, J., Webb, A.A., Locke, J., Schornack, S., Ajioka, J., Baulcombe, D.C., Zipfel, C., Kamoun, S., Jones, J.D., Kuhn, H., Robatzek, S., Van Esse, H.P., Sanders, D., Oldroyd, G., Martin, C., Field, R., O'Connor, S., Fox, S., Wulff, B., Miller, B., Breakspear, A, Radhakrishnan, G., Delaux, P.M., Loque, D., Granell, A, Tissier, A, Shih, P., Brutnell, T.P., Quick, W.P., Rischer, H., Fraser, P.D., Aharoni, A, Raines, C., South, P.F., Ane, J.M., Hamberger, B.R., Langdale, J., Stougaard, J., Bouwmeester, H., Udvardi, M., Murray, J.A, Ntoukakis, V., Schafer, P., Denby, K., Edwards, K.J., Osbourn, A, and Haseloff, J. (2015). Standards for plant synthetic biology: a common syntax for exchange of DNA parts. The New phytologist 208, 13-19.
Google Scholar: Author Only Title Only Author and Title

Pei, Z.M., Murata, Y., Benning, G., Thomine, S., Klusener, B., Allen, G.J., Grill, E., and Schroeder, J.I. (2000). Calcium channels activated by hydrogen peroxide mediate abscisic acid signalling in guard cells. Nature 406, 731-734.
Google Scholar: Author Only Title Only Author and Title

Roma, L.P., Deponte, M., Riemer, J., and Morgan, B. (2018). Mechanisms and applications of redox-sensitive green fluorescent protein-based hydrogen peroxide probes. Antioxidants & redox signaling 29, 552-568.
Google Scholar: Author Only Title Only Author and Title

Sasso, S., Stibor, H., Mittag, M., and Grossman, A.R. (2018). From molecular manipulation of domesticated Chlamydomonas reinhardtii to survival in nature. eLife 7.
Google Scholar: Author Only Title Only Author and Title

Schmidt, G.W., Matlin, K.S., and Chua, N.H. (1977). A rapid procedure for selective enrichment of photosynthetic electron transport mutants. Proceedings of the National Academy of Sciences 74, 610-614.
Google Scholar: Author Only Title Only Author and Title

Schroda, M. (2019). Good news for nuclear transgene expression in Chlamydomonas. Cells 8.
Google Scholar: Author Only Title Only Author and Title

Schroda, M., Hemme, D., and Mühlhaus, T. (2015). The Chlamydomonas heat stress response. Plant J. 82, 466-480.
Google Scholar: Author Only Title Only Author and Title

Schwarzlander, M., Dick, T.P., Meyer, A.J., and Morgan, B. (2016). Dissecting redox biology using fluorescent protein sensors. Antioxidants & redox signaling 24, 680-712.
Google Scholar: Author Only Title Only Author and Title

Schwarzlander, M., Wagner, S., Ermakova, Y.G., Belousov, V.V., Radi, R., Beckman, J.S., Buettner, G.R., Demaurex, N., Duchen, M.R., Forman, H.J., Fricker, M.D., Gems, D., Halestrap, A.P., Halliwell, B., Jakob, U., Johnston, I.G., Jones, N.S., Logan, D.C., Morgan, B., Muller, F.L., Nicholls, D.G., Remington, S.J., Schumacker, P.T., Winterbourn, C.C., Sweetlove, L.J., Meyer, A.J., Dick, T.P., and Murphy, M.P. (2014). The 'mitoflash' probe cpYFP does not respond to superoxide. Nature 514, E12-14.
Google Scholar: Author Only Title Only Author and Title

Strenkert, D., Schmollinger, S., and Schroda, M. (2013). Heat shock factor 1 counteracts epigenetic silencing of nuclear transgenes in Chlamydomonas reinhardtii. Nucleic Acids Res. 41, 5273-5289.
Google Scholar: Author Only Title Only Author and Title

Sun, A.Z., and Guo, F.Q. (2016). Chloroplast retrograde regulation of heat stress responses in plants. Frontiers in plant science 7, 398.
Google Scholar: Author Only Title Only Author and Title

Ugalde, J.M., Fuchs, P., Nietzel, T., Cutolo, E.A, Vothknecht, U.C., Holuigue, L., Schwarzländer, M., Müller-Schüssele, S.J., and Meyer, A.J. (2020). Chloroplast-derived photo-oxidative stress causes changes in H2O2 and EGSH in other subcellular compartments. bioRxiv, 2020.2007.2020.212670.
Google Scholar: Author Only Title Only Author and Title

Vacca, R.A, de Pinto, M.C., Valenti, D., Passarella, S., Marra, E., and De Gara, L. (2004). Production of reactive oxygen species, alteration of cytosolic ascorbate peroxidase, and impairment of mitochondrial metabolism are early events in heat shock-induced programmed cell death in tobacco Bright-Yellow 2 cells. Plant Physiol. 134, 1100-1112.
Google Scholar: Author Only Title Only Author and Title

Volkov, R.A, Panchuk, II, Mullineaux, P.M., and Schoffl, F. (2006). Heat stress-induced H2O2 is required for effective expression of

heat shock genes in Arabidopsis. Plant Mol. Biol. 61, 733-746.
Google Scholar: Author Only Title Only Author and Title

Waszczak, C., Carmody, M., and Kangasjarvi, J. (2018). Reactive oxygen species in plant signaling. Annu. Rev. Plant Biol. 69, 209-236.
Google Scholar: Author Only Title Only Author and Title

Weber, E., Engler, C., Gruetzner, R., Werner, S., and Marillonnet, S. (2011). A modular cloning system for standardized assembly of multigene constructs. PLoS One 6, e16765.
Google Scholar: Author Only Title Only Author and Title